ARR No. L4C16

NATIONAL ADVISORY COMMITTEE FOR AERONAUTICS

WARTIME REPORT

ORIGINALLY ISSUED

October 1944 as
Advance Restricted Report L4C16

COMPRESSIBILITY EFFECTS ON HEAT TRANSFER AND PRESSURE DROP IN SMOOTH CYLINDRICAL TUBES

By Jack N. Nielsen

Langley Memorial Aeronautical Laboratory
Langley Field, Va.

NACA

WASHINGTON

NACA ARR No. L4C16

NATIONAL ADVISORY COMMITTEE FOR AERONAUTICS

ADVANCE RESTRICTED REPORT

COMPRESSIBILITY EFFECTS ON HEAT TRANSFER AND PRESSURE DROP IN SMOOTH CYLINDRICAL TUBES

By Jack N. Nielsen

SUMMARY

An analysis is made to simplify pressure-drop calculations for nonadiabatic and adiabatic friction flow of air in smooth cylindrical tubes when the density changes due to heat transfer and pressure drop are appreciable. Solutions of the equation of motion are obtained by the use of Reynolds' analogy between heat transfer and skin friction. Charts of the solutions are presented for making pressure-drop calculations. A technique of using the charts to determine the position of a normal shock in a tube is described.

INTRODUCTION

The heat transfer and pressure drop for the flow of air in smooth cylindrical tubes may be calculated without difficulty only when the density changes that accompany the changes of temperature and pressure are relatively small. In the present paper an attempt is made to analyze flow with large density changes, such as occur at high Mach numbers, in order to simplify the calculation of such flow and to provide a basis for the correlation of data.

The analysis depends on the validity of Reynolds' analogy between heat transfer and skin friction, which leads to the equality of the heat-transfer and skin-friction coefficients. By means of this simplification the equation of motion can be solved for the nonadiabatic case and the stagnation-temperature variation along the tube can then be obtained as a function of the Mach number; the solution is given in the form of a chart. The adiabatic case, a limiting form of the nonadiabatic case, is also analyzed in some detail and the solution

for the pressure variation is given in graphical form. Some discussion is included of available experimental data (references 1 to 3) in order to evaluate the assumptions that are made herein and the applicability of the solutions.

SYMBOLS

T	absolute temperature, $^{\circ}F + 460$
x	distance in flow direction, feet
y	distance perpendicular to flow direction, feet
u	velocity in flow direction, feet per second
v	velocity perpendicular to flow direction, feet per second
k	thermal conductivity, $\frac{\text{Btu}}{\text{seconds} \times \text{feet}^2 \times {}^{\circ}F/\text{feet}}$
ρ	mass density, slugs per cubic foot
μ	absolute viscosity, $\frac{\text{slugs}}{\text{seconds} \times \text{feet}}$
Pr	Prandtl number (about 0.73 for laminar flow of air at room temperature) $(\mu c_p/k)$
T_s	stagnation temperature, $^{\circ}F + 460$
C_H	nondimensional heat-transfer coefficient
C_F	nondimensional skin-friction coefficient
D	tube diameter, feet
G	mass rate of flow per unit area, $\frac{\text{slugs}}{\text{feet}^2 \times \text{seconds}}$
Re	Reynolds number $\left(\frac{GD}{\mu}\right)$
p	static pressure, pounds per square foot

R gas constant, $\frac{\text{foot-pounds}}{\text{slugs} \times {}^{\circ}\text{F}}$ (about 1716 for air); also tube radius, feet

J mechanical equivalent of heat (778 foot-pounds per Btu)

c_p specific heat at constant pressure, $\frac{\text{Btu}}{\text{slugs} \times {}^{\circ}\text{F}}$

γ ratio of specific heats (taken as 1.404 for all figures)

M Mach number $\left(\frac{u}{\sqrt{\gamma RT}}\right)$

T_w wall temperature, $^{\circ}F + 460$

ϵ nondimensional temperature ratio (T_s/T_w)

r distance from tube axis, feet

A tube cross-sectional area, square feet

L tube length, feet

G_t isentropic mass flow per unit area in throat of supersonic nozzle, $\frac{\text{slugs}}{\text{feet}^2 \times \text{seconds}}$

K constant

Subscripts:

c tube center

o initial

1 before shock

2 after shock

s stagnation

A single bar over a symbol denotes an average with respect to cross-sectional area; a double bar denotes an average with respect to cross-sectional area with ρu as weighting factor.

REYNOLDS' ANALOGY

Reynolds' analogy between heat transfer and skin friction involves a similarity of velocity and temperature fields. For steady low-speed flow of air along a flat plate, the velocity and temperature fields are given by the simplified boundary-layer equations

$$u\frac{\partial T}{\partial x} + v\frac{\partial T}{\partial y} = \frac{k}{\rho c_p}\frac{\partial^2 T}{\partial y^2}$$

and

$$u\frac{\partial u}{\partial x} + v\frac{\partial u}{\partial y} = \frac{\mu}{\rho}\frac{\partial^2 u}{\partial y^2} \qquad (1)$$

If the Prandtl number $\mu c_p/k$ is unity and if the plate is at uniform temperature T_w, the $(T - T_w)$-field and the u-field are similar, since their differential equations and boundary conditions are then identical. For laminar flow of air at ordinary temperatures the value of the Prandtl number is approximately 0.73. For turbulent flow, however, the effective values of μ and k are increased because of the net turbulent interchange of momentum and heat, respectively. The Prandtl number for turbulent flow will vary somewhat with position because, on the basis of mixing-length theory, the increase in the effective values of the thermal conductivity and the viscosity depend on the turbulent mixing length and the velocity gradient.

Measurements given in reference 3 show that the temperature and velocity profiles in the turbulent boundary layer along a flat plate at uniform temperature are nearly the same even though the boundary conditions of the temperature and velocity fields were not exactly identical during the measurements. The measurements indicate that the use of an average Prandtl number of unity for a turbulent boundary layer should not be greatly in error. The measurements in reference 4 also show that the effect of density gradients on the velocity profile may be neglected at moderately small temperature differences.

Reynolds' analogy may be directly extended to low-speed turbulent flow of air in tubes if the effects on the velocity profile of the pressure gradients due to skin friction and of the density gradients due to heat transfer may be disregarded. This assumption is justified by the good experimental agreement of the low-speed skin-friction and heat-transfer data in reference 5 with Reynolds' analogy.

The effect of compressibility on the velocity profile has been measured by Frössel (reference 2), who concludes that for subsonic adiabatic flow of air in smooth cylindrical tubes the velocity profile is not affected by compressibility. The effect of compressibility on the temperature profile may be seen from the following differential equation for two-dimensional motion of a compressible fluid in a boundary layer:

$$\frac{D}{Dt}\left(T + \frac{u^2}{2c_pJ}\right) = \frac{k}{\rho c_p}\frac{\partial^2}{\partial y^2}\left(T + Pr\,\frac{u^2}{2c_pJ}\right) \qquad (2)$$

Equation (2) is given by Goldstein in reference 6 and attributed by him to Busemann (reference 7). For $Pr = 1$ and for steady flow,

$$u\frac{\partial T_s}{\partial x} + v\frac{\partial T_s}{\partial y} = \frac{k}{\rho c_p}\frac{\partial^2 T_s}{\partial y^2} \qquad (3)$$

Comparison of equations (1) and (3) shows that for compressible flow the $(T_s - T_w)$-field and the u-field are similar for identical boundary conditions. For compressible flow Reynolds' analogy thus postulates the similarity of the stagnation-temperature and velocity fields. For incompressible flow this similarity reduces to the similarity of the $(T - T_w)$-field and the u-field.

Reynolds' analogy results in an equality of the nondimensional heat-transfer and skin-friction coefficients, which is the basis for the subsequent analysis. The nondimensional coefficients are given by the following expressions:

$$C_H = \frac{k\left[\frac{\partial(T_w - T_s)}{\partial y}\right]_{y=0}}{\overline{\rho u c_p (T_w - T_s)}} \qquad (4)$$

$$C_F = \frac{\mu\left(\frac{\partial u}{\partial y}\right)_{y=0}}{\overline{\rho u^2}} \qquad (5)$$

The single bar denotes an average with respect to cross-sectional area. The heat-transfer coefficient is the ratio of the heat transfer per unit area per unit time at the wall to the average total energy (relative to the energy where $T_s = T_w$) of the fluid flowing through unit cross-sectional area per unit time. The skin-friction coefficient is the ratio of the shearing stress at the wall to the average momentum of the fluid flowing through unit cross-sectional area per unit time. The similarity of the $(T_w - T_s)$-field and the u-field gives the following relationship:

$$\frac{\left[\frac{\partial(T_w - T_s)}{\partial y}\right]_{y=0}}{\overline{\rho u(T_w - T_s)}} = \frac{\left(\frac{\partial u}{\partial y}\right)_{y=0}}{\overline{\rho u^2}} \qquad (6)$$

From equations (4) to (6),

$$C_F = C_H$$

An experimental verification of this relationship for incompressible flow is given in reference 5 from the data of several investigators.

The value of C_F will vary with Reynolds number, roughness of tube wall, Mach number, shape of tube entrance, and distance from tube entrance. For adiabatic flow in smooth tubes beyond the entrance length in which the velocity profile is still changing, Frössel in reference 2 shows that C_F is independent of Mach number

up to the speed of sound and is given by the von Kármán-Nikuradse relationship

$$\frac{1}{\sqrt{8c_F}} = -0.8 + 2 \log Re \sqrt{8c_F} \qquad (7)$$

In computing the Reynolds number for the flow in a tube, the average air temperature may be used for evaluating the viscosity.

Pressure-drop and heat-loss measurements for hot air flowing through a water-cooled tube are reported in reference 1. For subsonic flow, it was found that Reynolds' analogy is independent of Mach number if the heat-transfer coefficients are calculated on the basis of the stagnation temperature and that the values of the skin-friction coefficient are in accord with formula (7).

Pressure-drop and heat-loss measurements for burned oil-air mixtures flowing through a smooth water-cooled tube at high temperatures and velocities are given in reference 8. The measurements are in good accord with Reynolds' analogy. It is also shown that, under the test conditions of reference 8, the skin-friction coefficients are given by the von Kármán-Nikuradse relationship for incompressible flow (equation (7)).

NONADIABATIC FRICTION FLOW

The equality of the heat-transfer and skin-friction coefficients given by Reynolds' analogy is used to reduce the differential equation of motion for compressible flow in a smooth tube at uniform wall temperature from three variables to two variables. The resulting equation is solved by the isocline technique to give a chart for making pressure-drop calculations. Particular attention is given to averaging the variables in the following derivation and solution of the equation of motion:

The differential equation of motion for uniform pressure at every cross section is

$$d\left(p + \overline{\rho u^2}\right) + \frac{4}{D} c_F \overline{\rho u^2}\, dx = 0$$

The variable $\overline{\rho u^2}$ is eliminated by introducing the average squared Mach number

$$\overline{M^2} = \frac{1}{A}\int_0^A M^2 \, dA$$

$$= \frac{1}{A}\int_0^A \frac{\rho u^2}{\gamma p} \, dA$$

$$= \frac{\overline{\rho u^2}}{\gamma p} \tag{8}$$

which gives

$$d\left(p + \gamma p\overline{M^2}\right) + \frac{4}{D}C_F \gamma p \overline{M^2} \, dx = 0$$

or, in different form,

$$\frac{1}{2}\left(\frac{1}{\gamma M^2} + 1\right) d\log p^2 + d\log \overline{M^2} + \frac{4}{D}C_F \, dx = 0 \tag{9}$$

The term $\frac{4}{D}C_F \, dx$ is replaced with a nondimensional temperature ratio by equating the differential heat transfer from the wall to the differential heat gained by the fluid; that is,

$$C_F \, \overline{\rho u(T_w - T_s)} \, c_p \pi D \, dx = c_p \frac{\pi D^2}{4} \, d\overline{\rho u T_s}$$

$$\frac{4}{D}C_H\,dx = \frac{d\,\overline{\rho u T_s}}{\rho u(T_w - T_s)}$$

$$= \frac{d\,\bar{\bar{\epsilon}}}{1 - \bar{\bar{\epsilon}}}$$

$$= 4\frac{C_F}{D}\,dx \qquad (10)$$

The double bar denotes an average with respect to cross-sectional area with ρu as weighting factor. Introducing the last equality of equation (10) in equation (9) gives

$$\frac{1}{2}\left(\frac{1}{\gamma \bar{M}^2} + 1\right) d\log p^2 + d\log \bar{M}^2 - d\log(\bar{\bar{\epsilon}} - 1) = 0 \qquad (11)$$

The last step in the derivation is to replace $\log p^2$ with an expression in $\bar{\bar{\epsilon}}$ and $\bar{M}^2$. With the aid of the relationships

$$p = \rho RT \qquad \epsilon = \frac{T_s}{T_w}$$

$$T_s = T\left(1 + \frac{\gamma - 1}{2} M^2\right) \qquad M^2 = \frac{u^2}{\gamma RT}$$

p^2 is expressed as

$$p^2 = \rho^2 u^2 \frac{RT_w}{\gamma} \frac{\epsilon}{M^2\left(1 + \frac{\gamma - 1}{2} M^2\right)} \qquad (12)$$

The transformation to an expression in $\bar{\bar{\epsilon}}$ and $\bar{M}^2$ depends on the considerations that the density and

velocity profiles are given by the ϵ- and M^2-profiles, since

$$\rho = \frac{p}{RT}$$

$$T = T_w \frac{\epsilon}{1 + \frac{\gamma - 1}{2} M^2}$$

and

$$u^2 = \gamma RTM^2$$

These considerations, in conjunction with equations (9) and (10), show that $\bar{T}$ and $\bar{M}^2$ depend only on the ϵ- and M^2-profiles, so that equation (12) may be written

$$p^2 = K \frac{\bar{\epsilon}}{\bar{M}^2\left(1 + \frac{\gamma - 1}{2} \bar{M}^2\right)} \frac{\gamma^2 p T_w}{\gamma} \qquad (13)$$

where the constant K, close to unity, depends only on the ϵ- and M^2-profiles, or on $\bar{\epsilon}$ and $\bar{M}^2$.

The constant K has been evaluated for the one-seventh power velocity profile, which is characteristic of fully developed turbulent flow, given by

$$u = u_c \left(1 - \frac{r}{R}\right)^{1/7}$$

and for the corresponding similar stagnation-temperature profile, given by

$$1 - \epsilon = (1 - \epsilon_c)\left(1 - \frac{r}{R}\right)^{1/7}$$

The evaluation of K introduces no particular mathematical difficulties but is tedious. The values are plotted in figure 1 against $\overline{M^2}$ for several values of $\overline{\epsilon}$. From figure 1 the variation of K with $\overline{M^2}$ and $\overline{\epsilon}$ is seen to be second order and will be neglected. The variation of K from the values of figure 1 for a fully developed velocity profile to a value of unity for a plane velocity profile is small; therefore K will hereafter be taken constant at unity. Taking K constant is equivalent to assuming one-dimensional flow, where $\overline{\epsilon}$ and $\overline{M^2}$ are significant averages.

With the simplification that K is constant, equation (13) may be written

$$\log p^2 = \log \frac{K G^2 R T_r}{\gamma} + \log \overline{\epsilon} - \log\left[\overline{M^2}\left(1 + \frac{\gamma - 1}{2}\overline{M^2}\right)\right]$$

or, in differential form,

$$d\log p^2 = d\log \overline{\epsilon} - d\log\left[\overline{M^2}\left(1 + \frac{\gamma - 1}{2}\overline{M^2}\right)\right] \qquad (14)$$

Finally, introducing equation (14) in equation (11) gives the desired differential equation of motion in $\overline{\epsilon}$ and $\overline{M^2}$, which is

$$\frac{d\overline{\epsilon}}{d\overline{M^2}} = \frac{\overline{\epsilon}\left(\overline{\epsilon} - 1\right)\left(\overline{M^2} - 1\right)}{\overline{M^2}\left(1 + \frac{\gamma - 1}{2}\overline{M^2}\right)\left[\gamma\overline{M^2} + 1 + \overline{\epsilon}\left(\overline{M^2} - 1\right)\right]} \qquad (15)$$

Equation (15) may be regarded as a differential form of the equation of motion when the conditions of Reynolds' analogy are fulfilled. Solutions were obtained by the isocline technique because a closed solution was not found. The resulting curves are shown in figure 2. The lower family of curves, for $\bar{\epsilon} < 1$, corresponds to heating of the fluid; the upper family of curves, for $\bar{\epsilon} > 1$, corresponds to cooling of the fluid. If $\bar{\epsilon} > 1$, $\bar{\epsilon}$ decreases along the tube; and, if $\bar{\epsilon} < 1$, $\bar{\epsilon}$ increases along the tube. For subsonic entrance Mach numbers, the local Mach number increases with tube length to the limiting value of unity and, for supersonic entrance Mach numbers, the local Mach number decreases with tube length to the limiting value of unity. In order that a solution pass continuously through a Mach number of unity, the value of $\bar{\epsilon}$ would have to increase for the upper set of curves, for which the fluid is already hotter than the wall, and would have to decrease for the lower set of curves, for which the fluid is already colder than the wall. Inasmuch as such changes are contrary to the second law of thermodynamics, the local Mach number may not pass continuously through unity.

In figure 2 some experimental data from reference 1 are included for comparison with the theoretical curves. The tube-wall temperature was not uniform for the experiment; therefore the data have been plotted for two separate intervals of tube length with the tube-wall temperature over each interval constant at its average value. The agreement between the theoretical and experimental results is close. Smooth curves instead of experimental points are given in figure 2 because the experimental points in figures 3 and 4 of reference 1 are connected by smooth curves.

In order to make more accurate pressure-drop calculations for heat exchangers, diagrams of $\bar{\epsilon}$ plotted against $\left(\frac{}{}\right)^{1/2}$ enlarged from figure 2 are given in figure 3(a) for subsonic heating and in figure 3(b) for subsonic cooling. The curves of figure 3 were obtained by taking the curves of figure 2 as first approximations. Special accuracy was attained in the curves by adjusting them so that the integral of the slope along each curve between any two points

$$\int_1^2 \frac{d\bar{\bar{\epsilon}}}{d\left(\overline{M^2}\right)^{1/2}} d\left(\overline{M^2}\right)^{1/2}$$

as given by equation (15), equaled the difference in ordinates between the two points on the curve.

By equation (13), with γ constant,

$$\frac{p}{p_o} = \frac{\left[\dfrac{\bar{\bar{\epsilon}}}{\overline{M^2}\left(1 + \dfrac{\gamma - 1}{2}\overline{M^2}\right)}\right]^{1/2}}{\left[\dfrac{\bar{\bar{\epsilon}}_o}{\overline{M_o^2}\left(1 + \dfrac{\gamma - 1}{2}\overline{M_o^2}\right)}\right]^{1/2}} \qquad (16)$$

In order to simplify pressure-drop calculations, lines of constant

$$\left[\frac{\bar{\bar{\epsilon}}}{\overline{M^2}\left(1 + \dfrac{\gamma - 1}{2}\overline{M^2}\right)}\right]^{1/2}$$

have been plotted in figure 3(a) and designated lines of constant relative pressure. In making a pressure-drop calculation, the value of this expression for the final condition is divided by the value for the initial condition to give p/p_o. A résumé of the procedure follows.

The value of $\bar{\bar{\epsilon}}_o$ for the initial point is found from the values of the tube-wall temperature T_w and the initial stagnation temperature $\bar{T}_s$, which either are known or may be measured. The value of $\left(\overline{M_o^2}\right)^{1/2}$ for the initial point is calculated from equation (13) for values of G, T_w, and p_o, which either are known or may be measured. The values of $\bar{\bar{\epsilon}}_o$ and

$\left(\overline{M_o^2}\right)^{1/2}$ locate the initial point in figure 3. The final point is located by following the curve of the solution through point $\bar{\bar{\epsilon}}_o$, $\left(\overline{M_o^2}\right)^{1/2}$ to the final value of $\bar{\bar{\epsilon}}$. This value of $\bar{\bar{\epsilon}}$ is obtained from an integration of equation (10) by assuming C_H constant at its average value; thus,

$$\bar{\bar{\epsilon}} = 1 + \left(\bar{\bar{\epsilon}}_o - 1\right)e^{-4C_H \frac{L}{D}} \tag{17}$$

The values of C_H for fully developed turbulent flow in smooth tubes, as given by equation (7), are plotted in figure 4. For the entrance length of a tube in which the velocity profile is changing, the value of C_H varies along the tube and depends on the entrance conditions, which determine the initial velocity profile. If experimental values of C_H for specific entrance conditions are not available, the value of C_H given by figure 4 may be used as the average value for the tube with the interpretation that this value will be slightly low. Finally, for the initial and final points now located in figure 3 the initial and final values of

$$\left[\frac{\bar{\bar{\epsilon}}}{\overline{M^2}\left(1 + \frac{\gamma - 1}{2}\overline{M^2}\right)}\right]^{1/2}$$

are determined with the help of the lines of constant relative pressure, and the pressure ratio p/p_t is calculated by equation (16).

As an example, suppose the following values are known:

$\bar{\bar{\epsilon}}_o = 0.50$ $\quad$ $Re = 10^5$

$G = 1.0$ $\quad$ $\frac{L}{D} = 60$

$T_w = 760^\circ$ F abs. $\quad$ $p_o = 2070$ lb/sq ft

Equation (13) gives

$$\overline{M_o^2}\left(1 + \frac{\gamma - 1}{2}\overline{M_o^2}\right) = \frac{0.5 \times (1)^2 \times 1716 \times 760}{1.404 \times (2070)^2}$$

and

$$\left(\overline{M_o^2}\right)^{1/2} = 0.325$$

If the average value of C_H for the tube is taken as 0.00225 from figure 4, the value of $\bar{\bar{\epsilon}}$ computed from equation (17) is

$$\bar{\bar{\epsilon}} = 1 + (0.5 - 1)e^{-4(0.00225)(60)}$$

$$= 0.709$$

Following the curve in figure 3 through the point 0.325, 0.500 to $\bar{\bar{\epsilon}} = 0.709$ locates the point corresponding to tube exit.

The values of $\left[\dfrac{\bar{\bar{\epsilon}}_o}{\overline{M_o^2}\left(1 + \frac{\gamma - 1}{2}\overline{M_o^2}\right)}\right]^{1/2}$ and

$\left[\dfrac{\bar{\bar{\epsilon}}}{\overline{M^2}\left(1 + \frac{\gamma - 1}{2}\overline{M^2}\right)}\right]^{1/2}$ as given by the lines of constant

relative pressure are 2.14 and 1.66, respectively; therefore

$$\frac{p}{p_0} = \frac{1.66}{2.14}$$

$$= 0.775$$

The static pressure at the end of the tube is 77.5 percent of the static pressure at the tube entrance.

As previously mentioned, the average value of C_m for the tube is slightly higher than the value given by figure 4 because of the undeveloped flow in the entrance length; therefore, slightly larger values of $\bar{\epsilon}$ and of pressure drop than the foregoing may be anticipated. Curves for constant values of

$$\left[\frac{\bar{\epsilon}}{\overline{M^2}\left(1 + \frac{\gamma - 1}{2}\overline{M^2}\right)}\right]^{1/2}$$

are plotted in figure 5 over the range of $\left(\overline{M^2}\right)^{1/2}$ for which an accurate determination is not possible from figure 3.

Calculations may be made for tubes of nonuniform wall temperature by performing the calculation for several intervals of the length on the assumption that the tube-wall temperature is uniform at its average value over each interval. The validity of the preceding analysis for $M > 1$ may not be determined until experimental data on Reynolds' analogy are available for supersonic flow.

ADIABATIC FRICTION FLOW

The preceding analysis for noradiabatic friction flow includes adiabatic friction flow as a special case. The equation of motion for the adiabatic case is

obtained from equation (15) by letting $\bar{\bar{\epsilon}} = 1$. The assumption that $\bar{\bar{\epsilon}} = 1$ is based on the experimental observation that for adiabatic flow of air the tube wall is uniformly at stagnation temperature. Further, equation (3) for the stagnation-temperature field is in accord with this observation, since the particular solution

$$T_s = \text{Constant}$$

corresponds to no heat transfer.

The reduction of the equation of motion (equation (15)) to the adiabatic case proceeds as follows:

From equation (10),

$$\frac{d\bar{\bar{\epsilon}}}{(\bar{\bar{\epsilon}} - 1)} = -\frac{4}{D} C_F \, dx$$

When this expression is introduced in equation (15), together with $\bar{\bar{\epsilon}} = 1$, the resulting equation is

$$-4C_F \frac{dx}{D} = \frac{\left(\overline{M^2} - 1\right) d\overline{M^2}}{2\overline{M^2}\left(1 + \frac{\gamma - 1}{2}\overline{M^2}\right)}$$

Direct integration gives

$$4\int_0^{x/D} C_F \, d\frac{x}{D} = \frac{1}{2\gamma}\left(\frac{1}{\overline{M_o^2}} - \frac{1}{\overline{M^2}}\right) + \frac{\gamma + 1}{4\gamma} \log_e \frac{\overline{M_o^2}}{\overline{M^2}} \frac{1 + \frac{\gamma - 1}{2}\overline{M^2}}{1 + \frac{\gamma - 1}{2}\overline{M_o^2}} \quad (18)$$

The integral is retained in the solution because C_F may not always be assumed uniform along the tube. The variation of C_F will subsequently be discussed.

Equation (18), the solution of the equation of motion for adiabatic friction flow, is shown in figures 6(a) and 6(b) for two subsonic ranges of $\overline{M_o^2}$ and in figure 6(c) for a supersonic range of $\overline{M_o^2}$. As figures 6(b) and 6(c) show, a particular solution of equation (18) corresponds to a supersonic value of $\overline{M_o^2}$ as well as to a subsonic value of $\overline{M_o^2}$. These figures differ only in the lines of constant pressure ratio, which will be discussed.

The solutions are qualitatively like those for $\overline{\epsilon} < 1$ in figure 2. For subsonic values of $\overline{M_o^2}$ the local Mach number increases with tube length to a limiting value of unity, and for supersonic values of $\overline{M_o^2}$ the local Mach number decreases with tube length to the limiting value of unity. A real flow may not pass continuously through $\overline{M^2} = 1$ because

$$\frac{4}{D}\int_0^x C_F\,dx$$

is a maximum for this condition.

Before figure 6 may be used, the variation of C_F with Reynolds number, roughness of tube wall, Mach number, shape of tube entrance, and distance from tube entrance should be known. Frössel's data (reference 2) show that, for the range of Mach number less than unity, the velocity profile may not be fully developed until $L/D = 36$; and Keenan and Neumann (reference 3) found that C_F decreased along the tube until L/D was about 56. Beyond this entrance length, C_F may be considered constant. In figure 7 experimental data, taken from the results of reference 3 for flow beyond the entrance length, are compared with the theoretical solution of equation (18), C_F being taken constant at the value given by equation (7). The theoretical solution is in good agreement with the experimental data.

The conclusions of references 2 and 3 for the effect of compressibility on C_F at supersonic speeds are not in agreement. No effect of Mach number on C_F was found in reference 2 for tubes of $L/D \leq 25$. Reference 3 found a decrease in C_F with Mach number for tubes of $L/D \leq 46$ on the basis of data taken beyond an effective nozzle-pipe L/D of about 35 because of severe pressure fluctuations and possible variation of velocity profile in the entrance length. Further experiment may be necessary to isolate the compressibility effect and entrance effect on C_F for supersonic flow.

Curves of constant pressure ratio p/p_0 have been plotted in figure 5. The pressure ratios have been calculated from equation (16), reduced to

$$\left(\frac{p}{p_0}\right)^2 = \frac{\overline{M_0^2}}{M^2} \frac{1 + \frac{\gamma - 1}{2} \overline{M_0^2}}{1 + \frac{\gamma - 1}{2} M^2} \qquad (19)$$

In figures 6(a) and 6(b) the lines of constant pressure ratio are based on the subsonic value of $\overline{M_0^2}$ and are valid only to $M = 1$ because the flow may not become supersonic for subsonic entrance Mach numbers. In figure 6(c) the lines of constant pressure ratio are based on the supersonic value of $\overline{M_0^2}$ and are valid for the entire range of Mach number. The curves of figure 6(c) are also valid in the case of normal shock because the assumptions of equation (19) do not preclude shock.

As a numerical example to illustrate pressure-drop calculations, consider $\overline{M_0^2} = 0.2$, $Re = 10^5$, and $L/D = 60$. From figure 4, $C_F = 0.00225$. Taking C_F constant for the tube as in the example for nonadiabatic flow gives

$$\frac{4}{D}\int_0^L C_F\,dx = \frac{4L}{D}C_F$$

$$= 4 \times 60 \times 0.00225$$

$$= 0.54$$

From figure 6(a), $p/p_0 = 0.735$; thus the static pressure at the end of the tube is 73.5 percent of the static pressure at the entrance of the tube.

COMPRESSION SHOCKS

For supersonic entrance Mach numbers, small lengths of rapidly rising pressure may occur within the tube if the static pressure in the reservoir behind the tube falls within a certain range. The pressure disturbance can be formed by the superposition of a number of pressure disturbances originating in the downstream flow and traveling upstream to a point where their velocity of propagation is equal to the stream velocity. At this point the disturbances would come to rest and form a compression shock. The position of the shock in the tube will vary with the static pressure in the reservoir. Figure 6 may be used to determine the position of a normal shock with the help of the following theoretical relationship between the Mach numbers before and after the shock:

$$M_2^2 = \frac{2 + \bar{M}_1^2(\gamma - 1)}{2\bar{M}_1^2 - (\gamma - 1)} \qquad (20)$$

The bars are omitted from the foregoing equation because the shape of the velocity profile in front of and behind a pressure disturbance is not known and averages could not be evaluated.

Equation (20) has been plotted in figure 8. Several experimental points from Frössel's results show good accord with the theoretical curve. The Mach numbers for the experimental points have been computed from Frössel's

data, plotted in terms of G/G_t and p/p_s, by means of the following relationship:

$$M^2\left(1 + \frac{\gamma - 1}{2} M^2\right) = \frac{(G/G_t)^2}{(p/p_s)^2}\left(\frac{2}{\gamma + 1}\right)^{\frac{\gamma+1}{\gamma-1}} \qquad (21)$$

where G_t is the isentropic mass flow per unit area in the throat of the supersonic nozzle in front of the pipe. The nondimensional equation (21) was obtained by introducing the following expression for G_t in equation (13):

$$G_t^2 = \gamma p_s \rho_s \left(\frac{2}{\gamma + 1}\right)^{\frac{\gamma+1}{\gamma-1}}$$

The subscript s refers to the initial stagnation conditions of the flow. Prössel's pressure measurements were not made sufficiently close together to determine the precise shape of the pressure distribution at the shock. For purposes of determining the points of figure 6, a sharp discontinuity was assumed to exist.

An example to show the method for determining graphically the position of the normal shock is shown in figure 6(c). If a shock forms at any point in the supersonic region, the end point of the shock may be determined by moving horizontally to the subsonic Mach number given by figure 6. The locus of such end points corresponding to a given value of M_c^2 form a shock line, which is shown as a broken line in figure 6(c). From the end point of the shock, the flow follows the subsonic solution to the value of $4\int_0^{L/D} C_F \, d\left(\frac{x}{D}\right)$ for the tube exit. The exit static pressure is then given by the lines of constant pressure ratio. The paths of the solution for two positions of the shock are shown in figure 6(c). It may be seen that, as the exit pressure is lowered, the shock moves downstream. After the exit

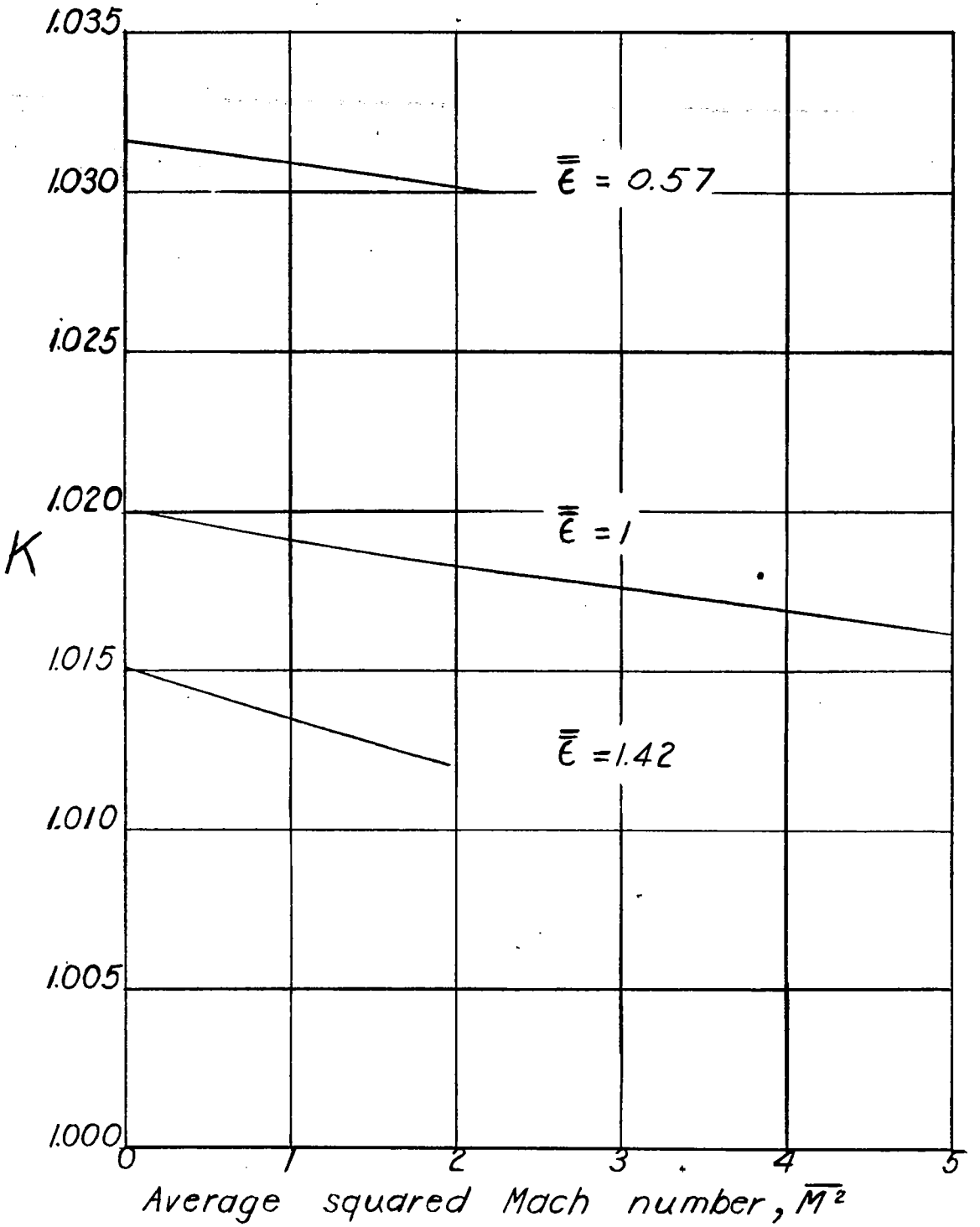

Figure 1.- Values of K from equation (13) for $\frac{1}{7}$-power velocity and stagnation-temperature profiles.

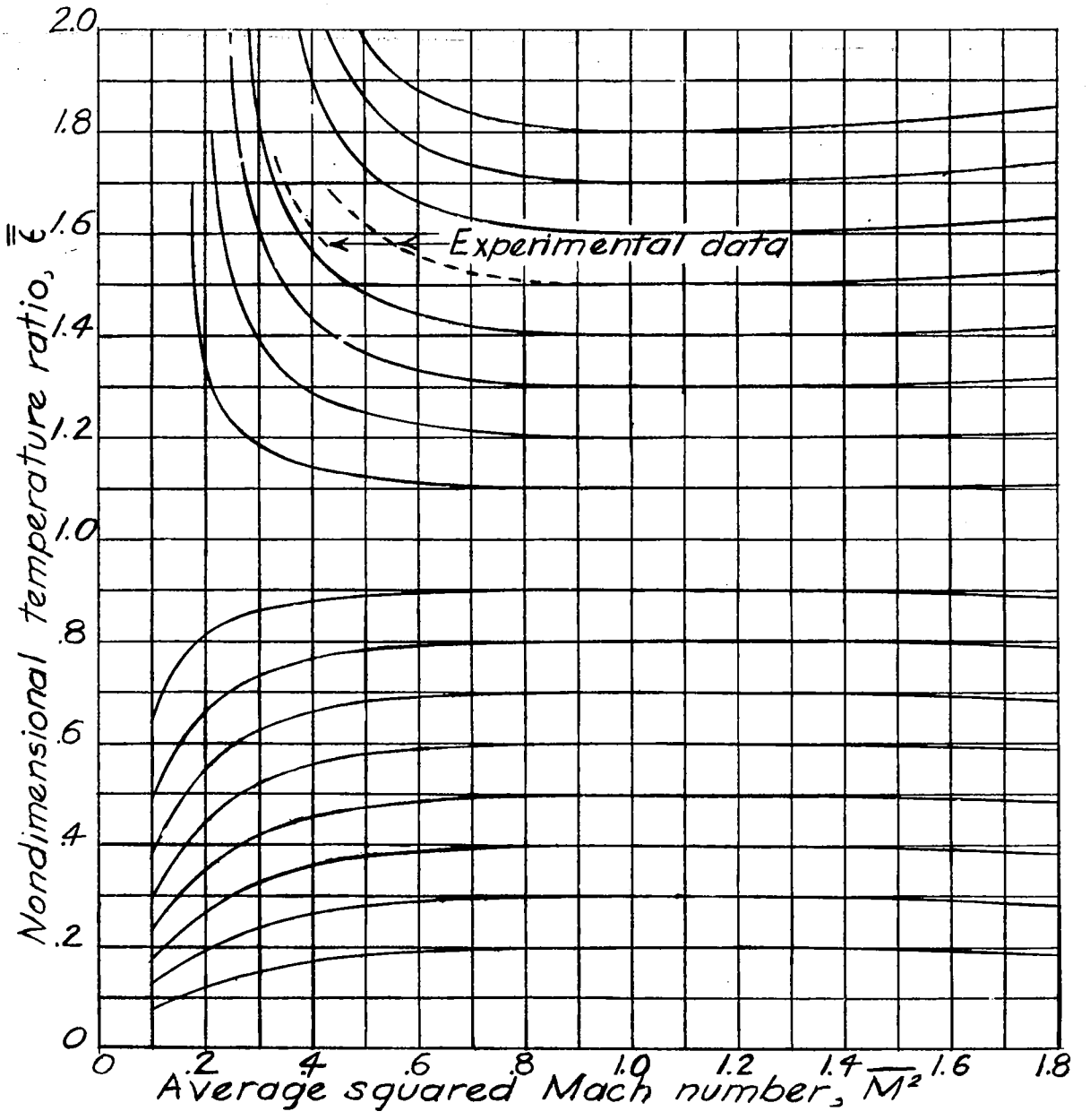

Figure 2.- General isocline solution of equation (15) for nonadiabatic friction flow in tubes at uniform wall temperature. (Experimental data from reference 1.)

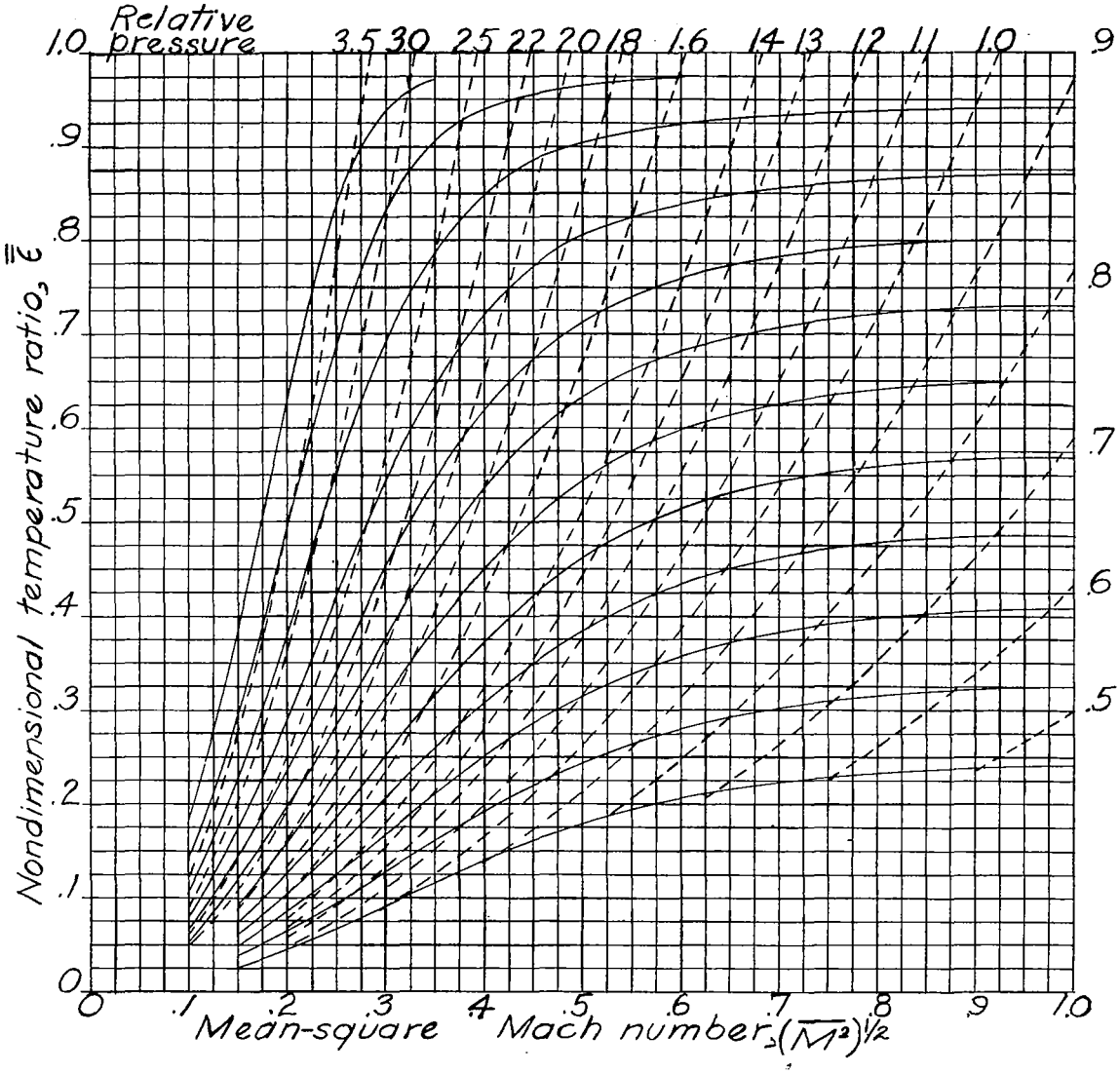

(a) Subsonic heating.

Figure 3.- Isocline solution of equation (15) for air in a tube at uniform wall temperature.

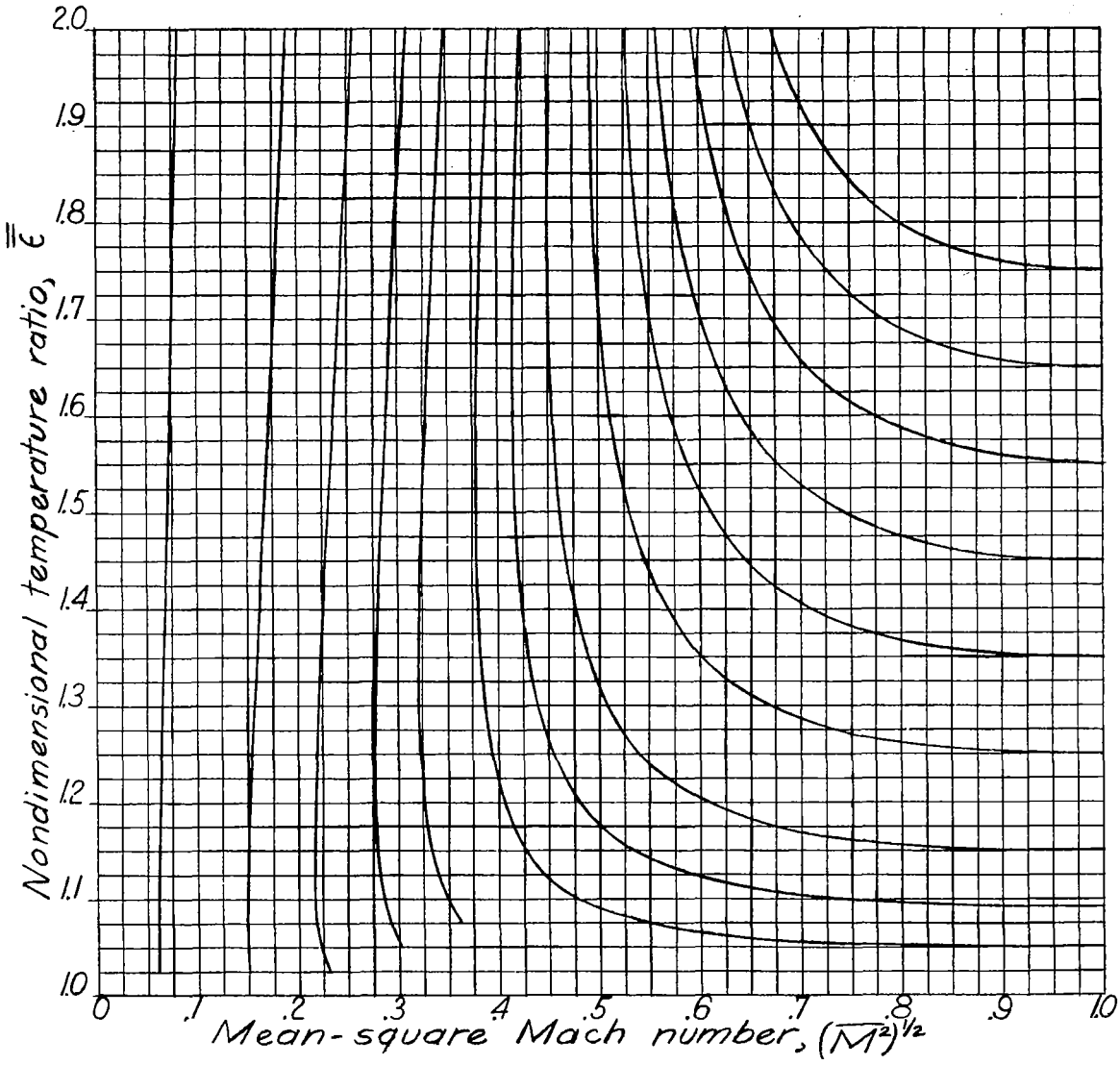

(b) Subsonic cooling.

Figure 3.- Concluded.

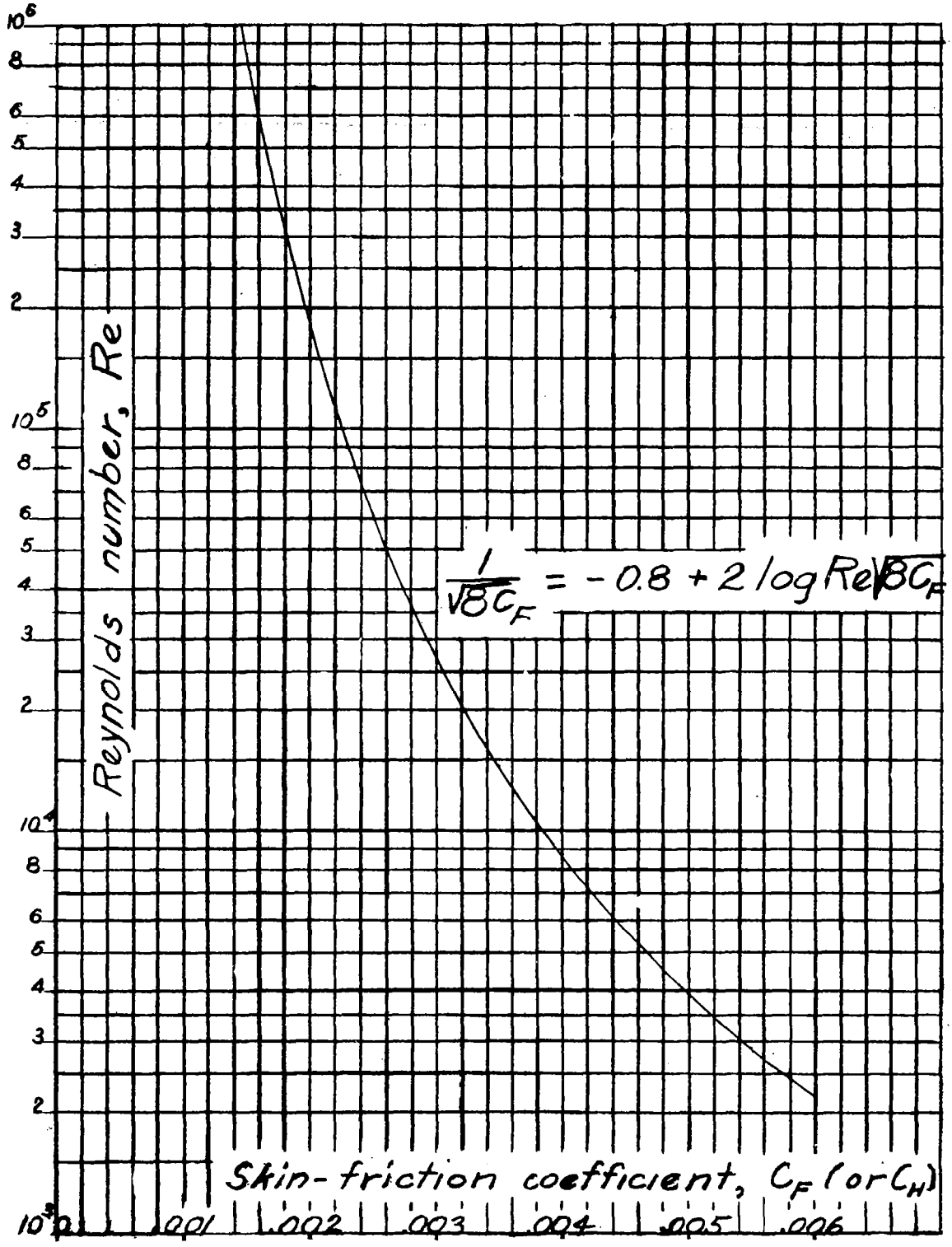

Figure 4.- Von Kármán-Nikuradse relationship between Reynolds number and skin-friction coefficient for flow in smooth tubes.

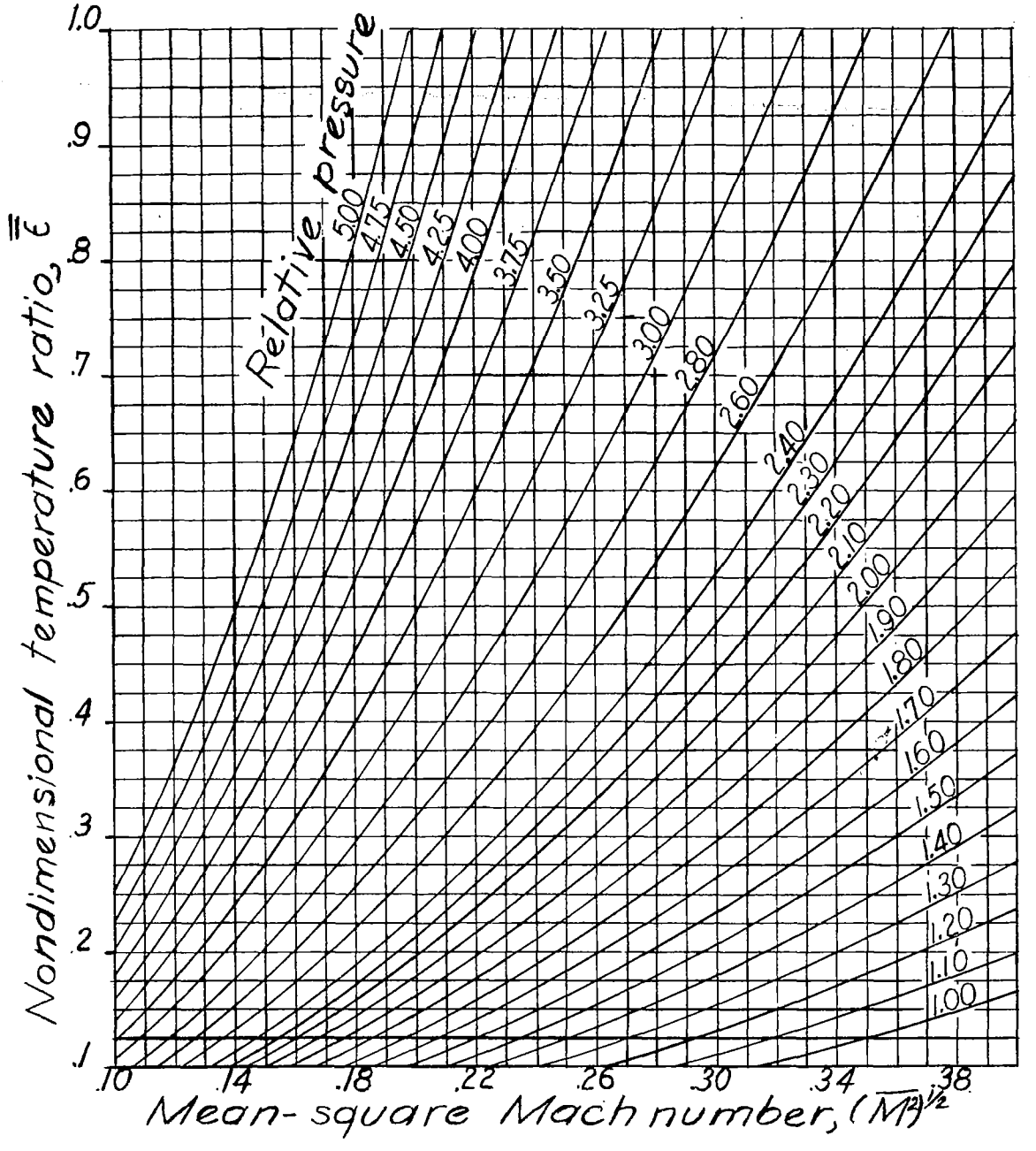

Figure 5.- Curves for constant $\left(\overline{M^2} \frac{\bar{\bar{\epsilon}}}{1 + \frac{\gamma - 1}{2} \overline{M^2}} \right)^{1/2}$ to be used with figure 3 for pressure-drop calculations.

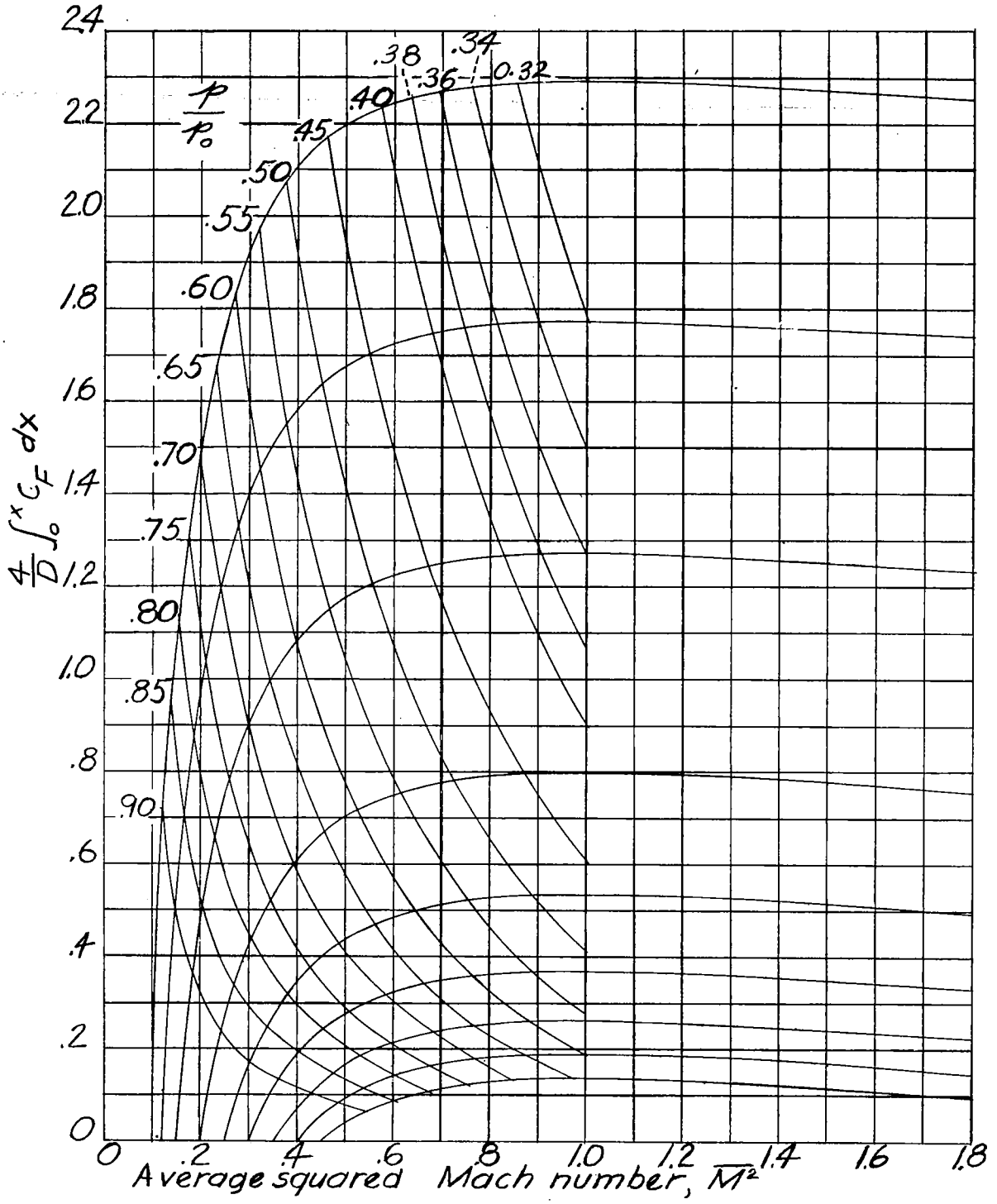

(a) Low range of subsonic entrance Mach numbers.

Figure 6.- Plot of equation (18) for adiabatic flow in smooth tubes.

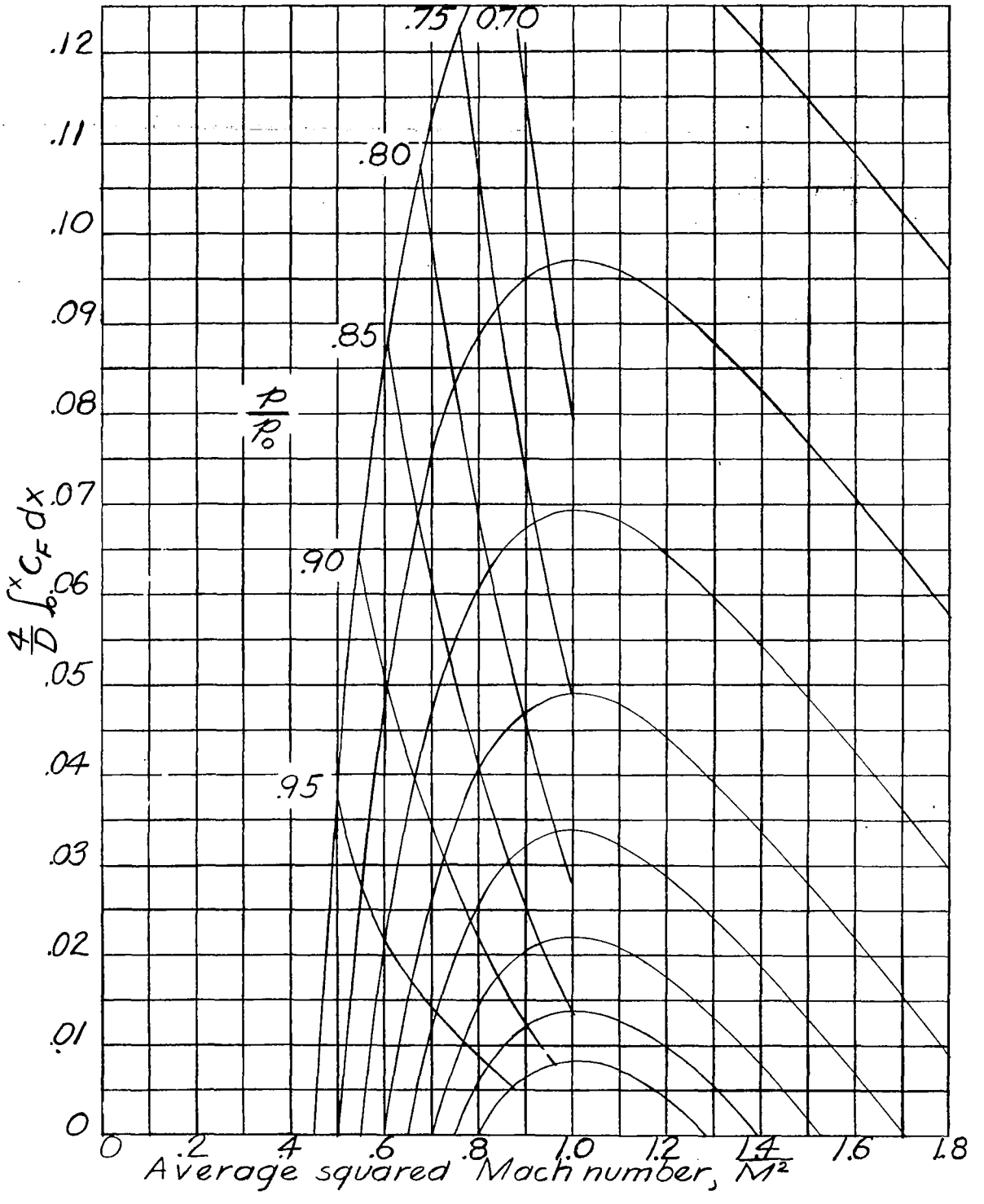

(b) High range of subsonic entrance Mach numbers.

Figure 6.- Continued.

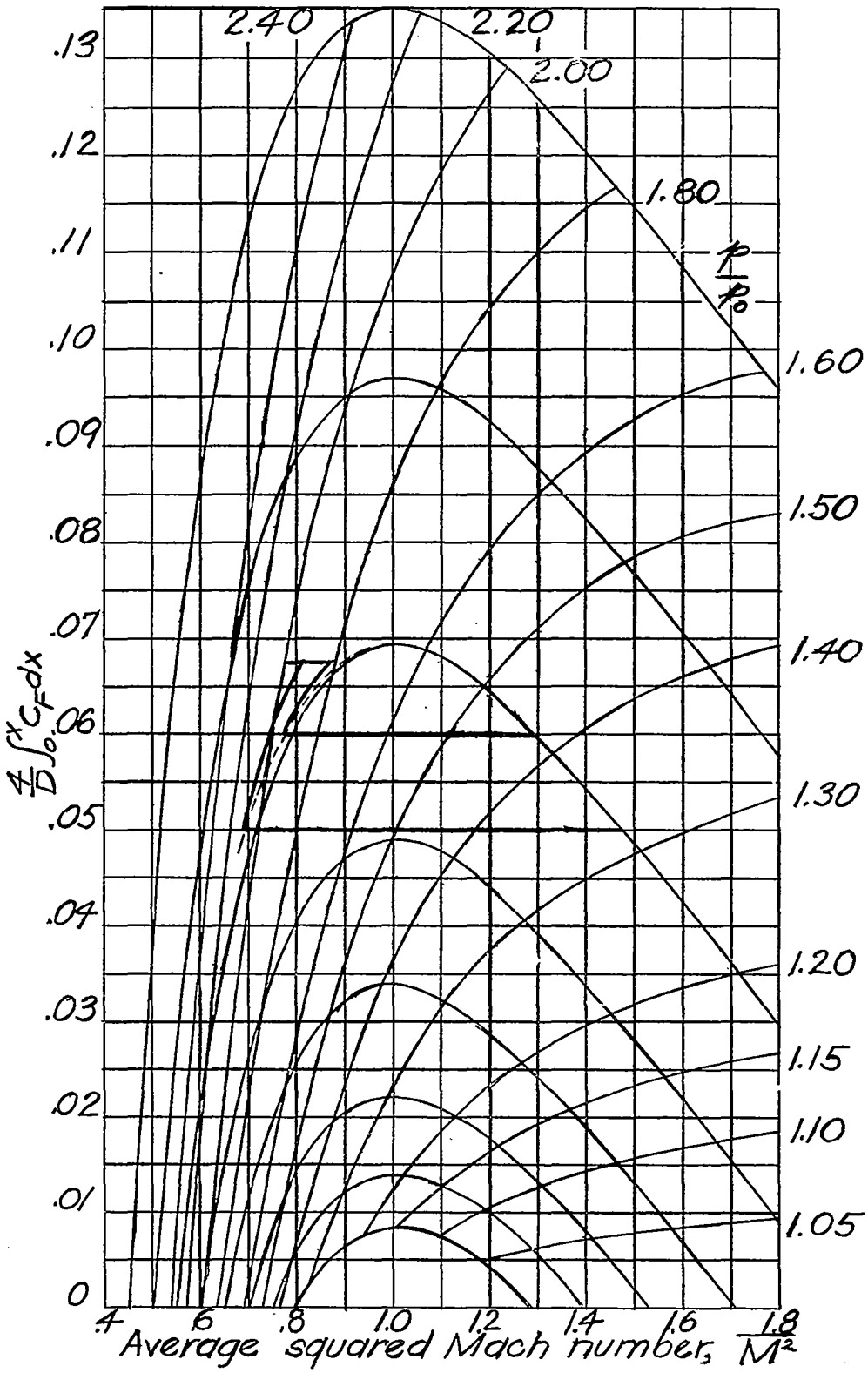

(c) Supersonic entrance Mach numbers.

Figure 6.- Concluded.

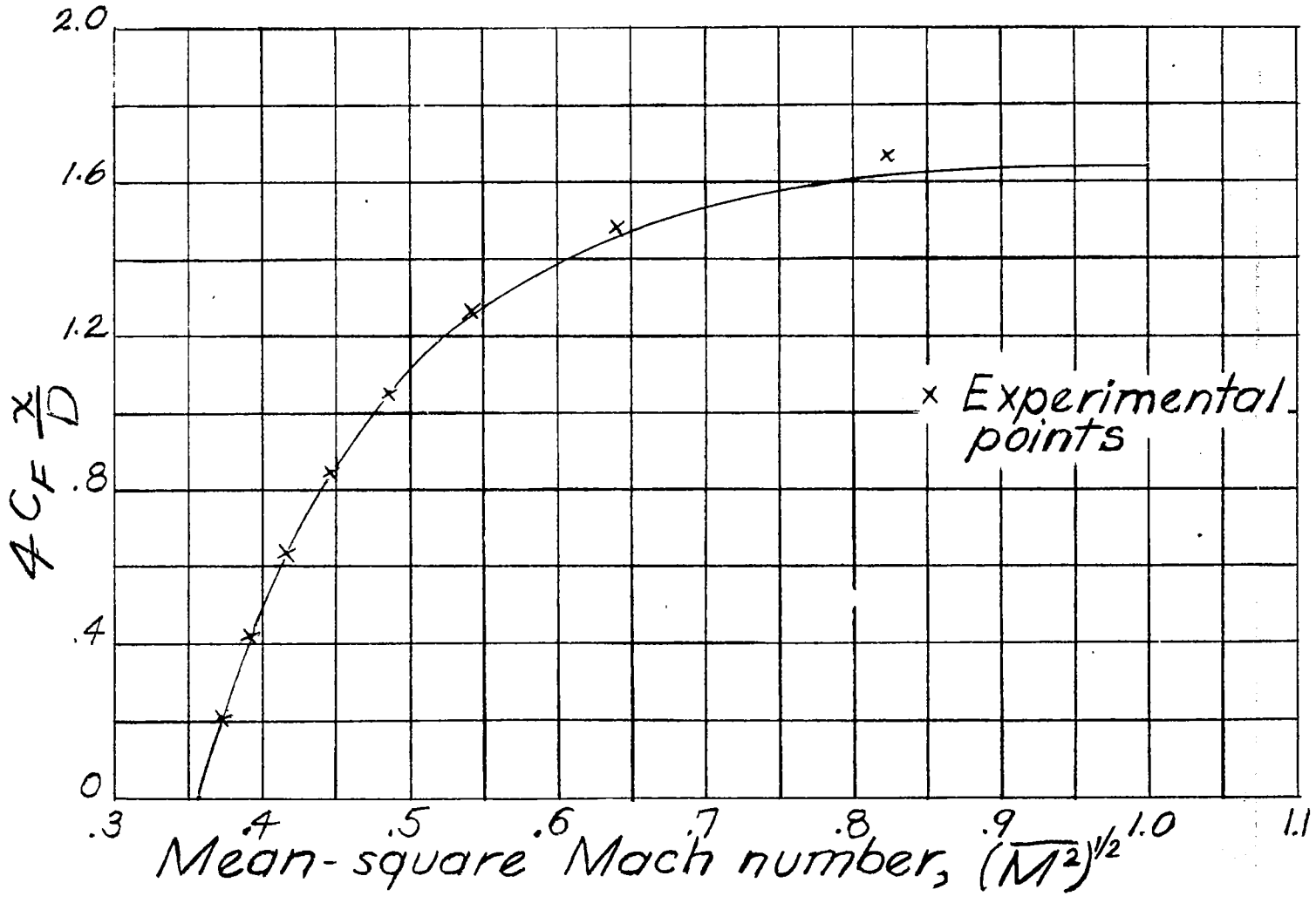

Figure 7.- Comparison of equation (18) with experimental data from reference 3.

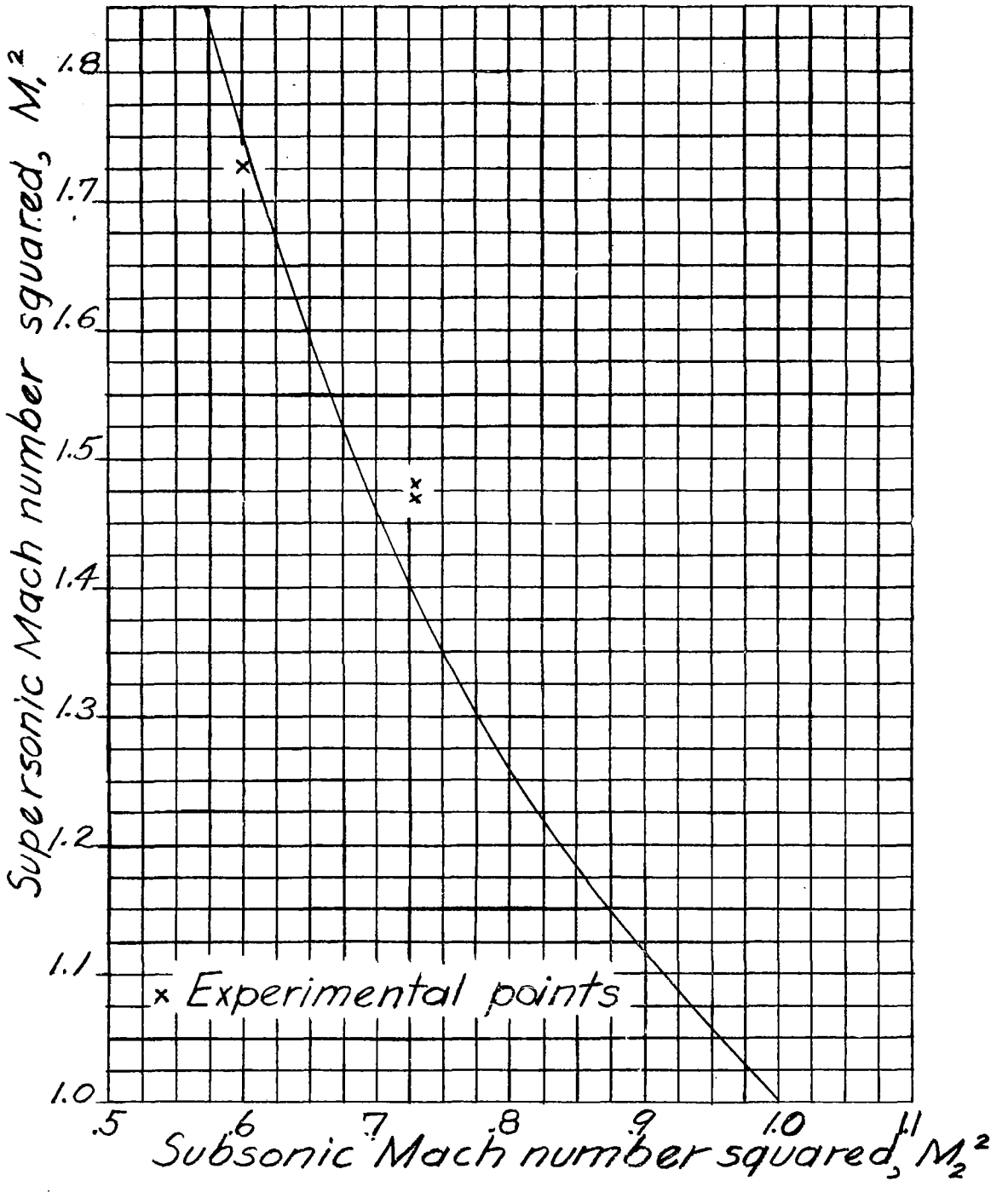

Figure 8.- Comparison of equation (20) with experimental data from reference 2.